ICAS 2021 SHANG HAI
32nd Congress of the International Council of the Aeronautical Sciences
September 6-10, 2021 Pudong Shangri-La, Shanghai, China

NONLINEAR UNSTEADY AERODYNAMIC MODELING AND LONGITUDINAL STABILITY ANALYSIS FOR AN AIRCRAFT MODEL

Yinan. Kong[1], Kaifeng. He[1], Mark H. Lowenberg[2], Simon A. Neild[2] & Fei. Cen[3]

[1]Computation Aerodynamics Institution, China Aerodynamics Research and Development Center, Mianyang, 621000, China
[2]Faculty of Engineering, University of Bristol BS8 1TR, UK
[3]Low speed Aeronautics Institution, China Aerodynamics Research and Development Center, Mianyang, 621000, China

Abstract

The high angle-of-attack region has become more accessible to modern aircraft due to advanced aerodynamic design giving improved control authority. In this regime, flow conditions change rapidly and flow separation and vortex breakdown can occur. At the same time, rapid angular rates will influence the flow state as well. Therefore, classical linear steady models are not suitable under these conditions, which increases the challenge in evaluating the overall stability and performance of aircraft. In this paper, a nonlinear mathematical modeling method based on the Goman-Khrabrov approach is used to capture aircraft aerodynamic characteristics influenced by unsteady phenomena such as flow separation. Bifurcation analysis of the resulting state-space system is proposed as a means of evaluating and interpreting the model. It is intended that, through this analysis method, phenomena such as limit cycle oscillations observed in wind tunnel tests can be explained. Experimental results from wind tunnel tests using the University of Bristol multi-degree-of-freedom 'maneuver rig' are used as a test case for this method. It is shown that the combination of a Goman-Khrabrov formulation and bifurcation analysis can be effective in developing models for predicting the stability of aircraft in the high angle-of-attack region or during rapid maneuvers.

Keywords: Unsteady aerodynamics; Bifurcation analysis; Dynamic test; High angle-of-attack

1. Introduction

Modern aircraft have high maneuver capabilities, and often fly at high angles-of-attack. However, wider flight envelopes and increased maneuverability bring new challenges to aerodynamic modeling, aircraft control and performance evaluation. For instance, because the flow condition changes rapidly, which is not only affected by incidence angle but also rotation rate, the aerodynamic model is not only nonlinear but also unsteady. These aerodynamic characteristics cause some unusual phenomena, such as multiple steady-state solutions, instabilities and oscillations. Examples of this behavior can be observed in wind tunnel tests, an example of which is the uncommanded pitching oscillations observed through dynamic testing of a model similar to a BAe Hawk trainer[1, 2]. This oscillatory phenomenon, characterized as a limit cycle oscillation (LCO), is an inherent dynamic feature of the aircraft dynamics under unsteady flow conditions. Note that this kind of limit oscillation of aircraft cannot be observed in a static wind tunnel test, a similar restriction arises in static numerical calculations. However such a response can be dangerous in an actual aircraft: large amplitude LCO could cause upset and even loss-of-control which remains the largest contributor to fatalities in civil aircraft accidents[2-5]. In the past, few aircraft models have included this operational region, those for highly maneuverable aircraft have flight at the high incidence nonlinear region but have not captured true time-dependency in flow phenomena. Nowadays, with the expansion of flight envelopes, including consideration of airliner loss-of-control, this is even more relevant. So there is a keen demand for researching unstable high angle of attack/high maneuver rate phenomena, predicting them and devising means of avoiding them.

As mentioned above, uncommanded pitching oscillations would not be observed in traditional wind tunnel experiments, to address this, special rigs are designed to physically simulate wind tunnel model motions allowing them to capture LCO and other responses. In the early 2000s, nonlinear behavior and limit cycle regions were observed through a pilot rig tested at the University of Bristol UK[1,2]. This focused on developing a control law to reduce or eliminate the LCO. At that time, the rig was a pendulum support system[6] - model mounted via a 2-degree-of-freedom (DOF) gimbal to the end of a pendulum arm suspended from above on a 3-DOF gimbal - and the modeling method devised for the control study wasn't generalized to different types of aircrafts.

The pendulum support rig was superseded by what is referred to as the 'maneuver rig': effectively a horizontal pendulum-based gimballed mechanism intended to allow a wider envelope of aircraft model maneuvers. Here too, unstable pitch motion of the same model can be observed[7-10]. To interpret this unstable characteristic, wind tunnel technology, aerodynamic mathematical concepts, parameter estimation techniques and bifurcation analysis can be combined to improve insight into the observed phenomena. In 2013, Pattinson used a two-point dynamic stall longitudinal model to depict the features of the high angle-of-attack region; bifurcation analysis was used to verify these methods in terms of parameter dependency of the nonlinear behavior [9]. The two-point modeling was based on the geometry of the sub-scale aircraft. Despite some success in identifying an unsteady model, there remained difficulties in specifying time characteristics for the system. This work demonstrated the validity of applying the Goman-Khrabrov (G-K) model[12] and, to some extent, the value of bifurcation analysis in informing the approach.

In order to understand aircraft dynamic features, other researchers also conducted dynamic wind tunnel tests based on different dynamic rigs. Rajamurthy built a single dynamic experimental setup to obtain comprehensive longitudinal aerodynamic data in the form of trim lift characteristics, dynamic stability derivatives, neutral point, and large-amplitude lift and pitching moment responses [13]; Peyada and Ghosh developed a parameter estimation method based on a wind tunnel device which is similar to the maneuver rig[14]; and descriptions of the dynamic wind tunnel facilities at NASA LaRC can be found in [15].

In terms of the Goman-Khrabrov model, it has been shown to be an effective method to represent unsteady characteristics e.g. modified indicial response method in conjunction with internal state-space was proposed by Huang for free-to-roll trajectory prediction[16], Williams used this method for pitching airfoil flow control[17], Fischenberg adopted this method to identify an unsteady aerodynamic stall model for the C-160 and VFW-614 ATTAS aircraft[18]. Other applications and transformation of the G-K model can be seen in [19-26]. Such applications of the G-K model demonstrate its ability to capture and predict aircraft upset phenomena. In this paper, further applications of the G-K model are investigated with an emphasis on extending the use of bifurcation analysis to fit the model parameters. Extensive use is made of longitudinal limit cycle oscillation data for an approximate BAe Hawk model measured by the University of Bristol 'maneuver rig'.

The paper is structured as follows. In Sec. II the maneuver rig for dynamic wind tunnel testing is briefly presented. Sec. III introduces the G-K mathematical modeling method for unsteady and nonlinear characteristics of aircraft at high angles-of-attack. Nonlinear and unsteady modeling results for the BAe Hawk aircraft model are derived, with the adopted approach to identifying the time character parameters explained in Sec. IV. The techniques of continuation and bifurcation analysis are used to replicate the LCO which is observed through wind tunnel tests, and the analysis results are given in Sec. V. This is followed by the conclusions and outlook for the proposed modelling methodology.

2. The Maneuver Rig

There are many theoretical and experimental methods to determine the flight characteristics of a new aircraft, such as various wind tunnel experimental techniques, empirical computational methods, computational fluid dynamics (CFD) methods, and finally flight test itself [8, 9, 15, 16, 25]. Each of these methods has its own advantages and disadvantages. But no matter how advanced a

theoretical

calculation method is, there is still a need to verify the results and often the requirement to gain insight into physical flight mechanics phenomena, through wind tunnel test.

For deriving flight mechanics data for controllability and dynamic stability evaluation, a wide variety of dynamic rig configurations have been explored. Essentially, dynamic wind tunnel rigs can be classified into three categories: forced-motion rigs, free-flying wind tunnel models, and free-motion rigs, in which some degrees of freedom are restricted[7, 13, 15]. Forced-motion rigs are regarded as industry-standard dynamic rigs. However, because the model is moved with fixed control surfaces, the forces differ from those generated in real flight; it is therefore useful to allow some degree of unconstrained motion in order to gain more understanding of dynamic loads on a model[6, 7, 13, 15].

The pendulum support rig developed approximately 15 years ago at the University of Bristol[4] suffered limitations including inadequate heave motion and the new maneuver rig was designed to overcome these defects[7, 8]. The layout was conceived by Goman and implemented and developed at the University of Bristol. It incorporates an aircraft model mounted via a 3-DOF gimbal (providing model roll, pitch and yaw) on an arm that is supported via another 3-DOF gimbal (allowing arm roll, pitch and yaw) on a rigid vertical sting mounted below the tunnel floor. An aerodynamic compensator is fixed to the rear of the arm, comprising a set of wings with flapped symmetric airfoil surfaces in a cruciform configuration. The aircraft model and the compensator control surfaces are actuated. Both gimbals can be locked in 1, 2 or all DOFs, giving a variety of possible testing conditions[5]. Although up to six rig DOF are available, the maximum number of aircraft model DOFs is five: both gimbals provide components of roll, while there is no unconstrained fore-aft DOF.

The initial design was subsequently enhanced (extra degree of freedom in the aircraft model-mounted gimbal, giving 6 gimbal degrees of freedom in total, and revised electronics that allowed for improved data acquisition and both model and rig control)[25, 26]. Model angles, compensator and model control surface deflections and outputs from a model-mounted inertial measurement unit are transmitted wirelessly to a data acquisition PC outside the tunnel; a wired connection is used to transmit the encoder measurements of rig arm angles. The multi-DOF nature of the testing that can be carried out on the rig allows acquisition of data for identification of aerodynamic models formulated to account for time-dependant dynamics, such as the longitudinal and lateral-directional manifestation of effects of aerodynamic hysteresis[28].

The experimental data used in this paper are obtained from the most recent update to the maneuver rig at the University of Bristol in which a load cell is incorporated just below the model gimbal. It measures forces and moments with respect to all three axes. As with other instrumentation on the aircraft model and rig, it transmits signals wirelessly to the data acquisition PC. Although the loads are not directly measured at the aircraft gimbal centre – which is usually also the centre of gravity (C.G.) – the measurements can be transformed to calculate the loads at the C.G.

Figure. 1 is a schematic diagram of the rig showing vertical sting, the locations of the two gimbals and the aircraft model and aerodynamic compensator, and indicating the degrees of freedom.

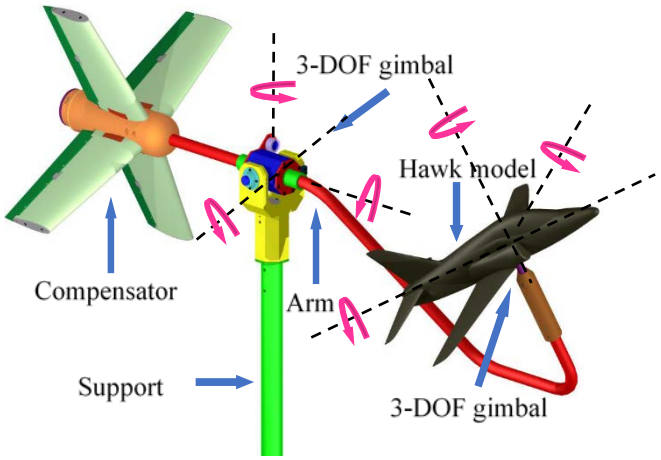

Figure 1 – the maneuver rig, 6-DOF (adapted from [8])

When the aircraft model generates sufficient lift to overcome the inertia of the arm it will begin to move; mass and/or aerodynamic balancing (using the compensator control surfaces) can be used to facilitate this[8]. In the absence of any compensation, movements of the arm would be influenced by the rig arm inertial properties, which is undesirable. Therefore, the function of the compensator is to attempt to compensate for the inertia and static forces generated by the mass of the arm (and other moving parts)[8, 10]; it can also be used to compensate for the lift and side force of the air vehicle to place it as appropriate in the tunnel, and for 'kinematic compensation' to match the motions more closely with an unconstrained model[11].

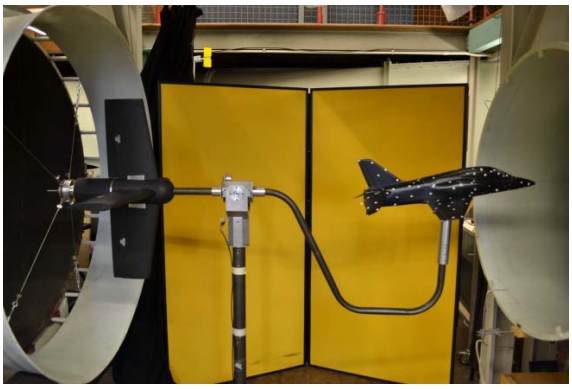

Figure 2 – Maneuver rig mounted in the open-jet section wind tunnel[5]

Figure.2 depicts the maneuver rig with the approximate Hawk model mounted in the University of Bristol's open-jet wind tunnel. The safety cable system attached to the rear of the arm is used to prevent the rig encountering dangerously large excursions [8]. The main geometric characteristics of Hawk model are given in Table 1.

Table 1 – Summary of Hawk model's geometric characteristics.

Physical parameter	Hawk model
Mean aerodynamic chord	0.143 m
Wing span	0.594 m
Mass	1.970 kg

3. Nonlinear Unsteady Modeling

A state-space representation of nonlinear unsteady aerodynamics was proposed by Goman & Khrabrov (1994), and has become a seminal work in the field of modeling unsteady aerodynamic behaviour Classical linear models are sufficiently accurate for attached flows but not under conditions where separated and vortex flow has developed [12]. The values of unsteady derivatives are strongly

dependent on the amplitude and frequency of aircraft oscillations, leading Goman & Khrabrov to introduce internal variables for describing the state of the flow. The resulting first- order differential equations describing the unsteady aerodynamics are convenient for flight dynamics applications as their form is simple and they can easily be appended to the aircraft motion equations[10, 12, 25]. This method is meaningful for aircraft stability analysis, since the state is an important concept for the description of dynamical systems. Thus the equations of motion of the aircraft include the dynamics of the unsteady flow representation and can be written as follows[12]:

$$\frac{\boldsymbol{dx}}{\boldsymbol{dt}} = \boldsymbol{f}(\boldsymbol{x}, \boldsymbol{h}); \boldsymbol{C} = \boldsymbol{g}(\boldsymbol{x}, \boldsymbol{h}) \tag{1}$$

Here x is a vector that approximately describes the state of separated and vortex flow of a wing. It is nondimensionalized $x \in [0,1]$ where $x = 1$ corresponds to fully attached flow , while $x = 0$ corresponds to leading-edge separation. The h vector contains the system inputs. The Hawk is a traditional configuration aircraft, so the airfoil has a sufficient thickness for the development of flow separation in the vicinity of the trailing edge. Wind tunnel test data and CFD results of the Hawk model showed that, the aerodynamics properties of these phenomena can be described in a similar way. For this, it is reasonable to use this model as the simplest approximation for the full aircraft, that is, that we can still use a similar approach for describing the aerodynamic characteristics of the Hawk at high angles of attack. Note that in this case the x does not corresponding to an exactly flow separation point any more, it become a generalized internal state variable which would not have the definite physical meaning. At first it is important to obtain the relations between the aircraft aerodynamic coefficients and the input parameters: the angle of attack α and the internal variable x [12]. From Gurevitch[29], the expression for the airfoil (with trailing-edge separation) nonlinear lift coefficient can be written as follows:

$$\boldsymbol{C_{L,m}^{nl}}(\boldsymbol{\alpha}, \boldsymbol{x}) = \boldsymbol{a_1}\left(\left(\boldsymbol{a_2} + \sqrt{\boldsymbol{x} - \boldsymbol{a_3}}\right)^2 + \boldsymbol{a_4}\right)\sin\boldsymbol{\alpha} + \boldsymbol{a_5} \tag{2}$$

The steady flow separation position is expressed as

$$\boldsymbol{x_0} = \boldsymbol{b_1}\tan^{-1}(\boldsymbol{\alpha} - \boldsymbol{b_2}) + \boldsymbol{b_3} \tag{3}$$

with the steady lift and moment coefficients given:

$$\boldsymbol{C_{L,m}^{st}}(\boldsymbol{\alpha}) = \boldsymbol{C_{L,m}^{st}}[\boldsymbol{\alpha}, \boldsymbol{x_0}(\boldsymbol{\alpha})] \tag{4}$$

The x_0 will cause stall at high angles-of-attack region.

Equation (4) defines the steady situation, i.e. the steady coefficient value in the absence of dynamics. An expression for the relationship in equation (4) can be obtained from static experiments or static calculations. Equations (2)-(4) are used here to describe the whole aircraft aerodynamic features, in which case x is a 'generalized internal state variable': it has no definite physical meaning but attempts to capture the dynamical properties associated with separation and/or vortex breakdown phenomena over the aircraft [11]. The unsteady aerodynamics of the approximate Hawk model are dominated by wing separation so that we retain the terminology adopted above for the airfoil modelling.

CFD or static wind tunnel test could produce steady aerodynamic data. Not only dynamic but also steady feature could be got from Maneuver rig, so it's more actuate to carry on dynamic analysis based on the data from the same wind tunnel facility. Through nonlinear aerodynamic modeling process, parameters $a_1 \sim a_5$ and $b_1 \sim b_3$in equation (2) and (3) can be determined. Note that equation (2) includes variable$x$, so the parameters in (2) and (3) should be estimated at the same time. Furthermore, in order to let the pitching moment coefficient curve has positive slope, the reference point has been transferred from C.G. of vehicle to horizontal tail direction, so that we could use the similar model structure to formula (2).

For unsteady flows the aerodynamic loads on an airfoil will depend on the current value of the angle of attack $\alpha(t)$ and instantaneous separation point position $x(t)$, which can differ considerably from its stationary value [12, 15]. The flow phenomena causing these differences can be divided into two groups. The first represents the quasi-steady effects (circulation and boundary layer convection lags as well as the so-called boundary layer improvement effect) which govern flow separation and reattachment; their combined effect is modelled via a delay on the quasi-steady position of the

separation point that is considered to be proportional to $\dot{\alpha}$. The second group of flow phenomena defines the dynamic properties of the separated flow adjustment – the transient aerodynamics effects: these flow relaxation dynamics are represented by a 1st-order differential equation. Therefore, the movement of the separation point for unsteady flow conditions[12, 19] can be described by:

$$\boldsymbol{\tau_1 \frac{dx}{dt} + x = x_0(\alpha - \tau_2 \dot{\alpha})} \tag{5}$$

Where τ_1 is the relaxation time constant governing the dynamic response (this parameter describes the decay of flow separation) and τ_2 is a time lag parameter, incorporating quasi-steady effects (this parameter describes the start time of separation or reattachment affected by unsteady motion). Essentially, $\tau_1$describes inherent features of an aircraft and τ_2 is related to its motion.

The closed mathematical model of aerodynamic lift coefficient for longitudinal motion is written as:

$$\begin{cases} \boldsymbol{C_L = C_L^{nl}(\alpha, x) + C_{L,q}^{att} \frac{qc}{V} + C_{L,\dot{\alpha}}^{att} \frac{\dot{\alpha} c}{V}} \\ \boldsymbol{\tau_1 \frac{dx}{dt} + x = x_0(\alpha - \tau_2 \dot{\alpha})} \end{cases} \tag{6}$$

The features of the mathematical model are illustrated in Figures. 3 and 4 for the parameters generated for the approximate Hawk. The effect of ramp motion on flow separation position is shown in Figure. 3, where the black solid line defines the steady dependency $x_0(\alpha)$; the blue lines show the variations of the separation point position for ramp motion with $\dot{\alpha} > 0$, the blue dashed line representing $\dot{\alpha} = 5 rad/s$ and blue dashed-dot line $\dot{\alpha} = 15 rad/s$; the red lines show the variations of the separation point position for ramp motions with $\dot{\alpha} < 0$, with the red dashed line denoting $\dot{\alpha} = -5 rad/s$ and red dashed dot-line $\dot{\alpha} = -15 rad/s$. When $\dot{\alpha} > 0$, unsteady effects postpone flow separation, and $\dot{\alpha} < 0$ postpones flow reattachment. Delay distance increases along with absolute value of $\dot{\alpha}$.

The appropriate variations of the lift coefficient with overshoot ($\dot{\alpha} > 0$) and undershoot ($\dot{\alpha} < 0$) are shown in the Figure. 4. Here, the black solid line expresses the steady lift coefficient; the dashed blue lines show the variations of lift coefficient for ramp motions with $\dot{\alpha} > 0$ (blue solid line represents $\dot{\alpha} = 10 rad/s$, blue dashed line $\dot{\alpha} = 20 rad/s$ and blue dashed-dot line $\dot{\alpha} = 30 rad/s$); the red lines show the variations of lift coefficient for ramp motions with $\dot{\alpha} < 0$ (red solid line denotes $\dot{\alpha} = -10 rad/s$, red dashed line $\dot{\alpha} = -20 rad/s$ and red dashed-dot line $\dot{\alpha} = -30 rad/s$). When $\dot{\alpha} > 0$, unsteady effects postpone flow separation, and $\dot{\alpha} < 0$ postpones flow reattachment. The green solid line represents the lift coefficient variation without "separation" ($x = 1$), and the green dashed line denotes lift coefficient value with total "separation" ($x = 0$). So the real lift value with "separation" effect will vary between the $x = 0$ and the $x = 1$ lines.

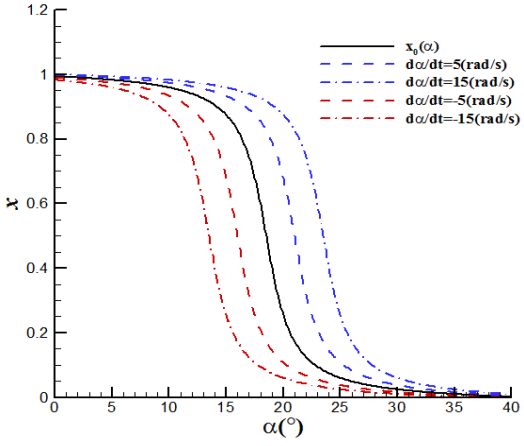

Figure 3 – Steady and unsteady separation point variation with α for Hawk model.

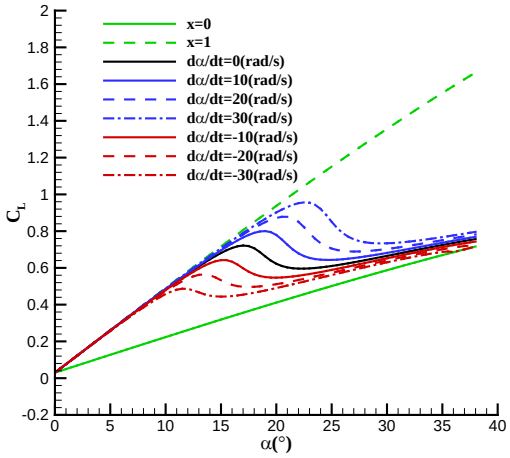

Figure 4 –Steady and unsteady lift coefficient of Hawk with trailing-edge separation

Similar characteristics can be achieved for the pitching moment coefficient. Thus, the mathematical model in the form of equations (2-4) and (6) are adopted to describe the main features of the

aerodynamics for both the lift and pitch moment observed in wind tunnel experiments. This mathematical model contains an unknown function$x_0(\alpha)$, and two unknown parameters, $\tau_1$andτ_2, which need to be defined from the steady and unsteady experimental data[12, 19]. The effect of ramp rate can be observed in Figures. 3 and 4. Time characteristics τ_1 and τ_2 have similar effects on aerodynamic coefficients, i.e. to postpone flow separation and reattachment.

Figure. 5 compares the variation with angle of attack of the modelled steady aerodynamic coefficients with the experimental data. The model matches the wind tunnel data satisfactorily in all three cases – lift, pitching moment and drag coefficients. From this diagram, the static flow separation process can be observed in the form of aerodynamic stall. For the drag coefficient, a polynomial representation is adopted, capturing the static variation with α, as this provides sufficient accuracy for subsequent analysis.

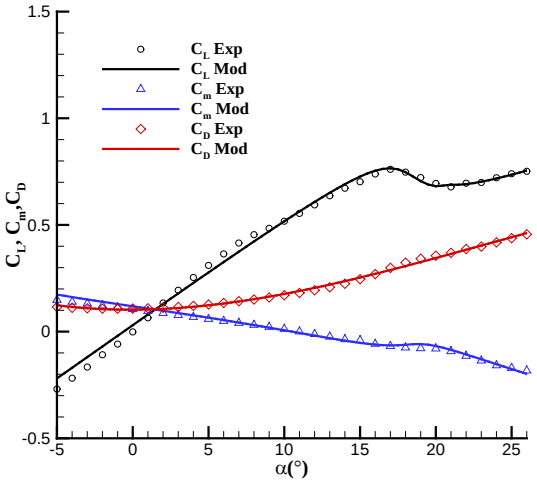

Figure 5 – Experimental and model lift, drag and pitching moment coefficients for Hawk model (V=30m/s)

4. Time Character Parameter Estimates

As mentioned above, the next step is to define the time character parameters, τ_1 and τ_2.

For the case of small amplitude forced oscillations, equations (6) can be used in the linearized form[12]. First, the right side of (6.b) is expanded with respect to α by using a 1st-order Taylor series:

$$x_0(\alpha - \tau_2\dot{\alpha}) = x_0(\alpha) + x_0`(\alpha)(-\tau_2\dot{\alpha}) \tag{7}$$

We define

$$\xi = x - x_0(\alpha), or\ x = \xi + x_0(\alpha) \tag{8}$$

Substitute (7) and (8) into (6.b), which can then be written as:

$$\tau_1 \frac{d\xi}{dt} + \xi = -(\tau_1 + \tau_2)\frac{dx}{d\alpha}\dot{\alpha} \tag{9}$$

Resorting to operator form

$$d/dt = s \tag{10}$$

then equation (9) can be written as:

$$\xi = -\frac{(\tau_1 + \tau_2)}{(\tau_1 s + 1)}\frac{dx_0}{d\alpha}\dot{\alpha} \tag{11}$$

Second, (6.a) is expanded at (α_0, x_0) by using a Taylor series：

$$C_L^{nl}(\alpha, x) = C_L^{nl}(\alpha_0, x_0) + \left(\frac{\partial C_L^{nl}}{\partial \alpha}(\alpha - \alpha_0) + \frac{\partial C_L^{nl}}{\partial x}(x - x_0)\right) + C_{Lq}\frac{qc}{V} + C_{L\dot{\alpha}}\frac{\dot{\alpha}c}{V} \tag{12}$$

For harmonic pitching oscillations, angle of attack changes as follows [29]:

$$\begin{cases} \alpha = \alpha_0 - \alpha_s \cos \omega \tau \\ \dot{\alpha} = \alpha_s \omega \sin \omega \tau \\ \ddot{\alpha} = \alpha_s \omega^2 \cos \omega \tau \end{cases} \quad (13)$$

Substitute $x - x_0 = \xi$ and $\alpha - \alpha_0 = -\alpha_s \cos \omega \tau$into (12) to obtain:

$$C_L^{nl}(\alpha,x) = a_1(a_2+\sqrt{a_2+x_0})^2\, sin\,\alpha_0 + a_1(a_2+\sqrt{a_3+x_0})^2\, cos\,\alpha_0\,(\alpha_s\, sin\,\omega\, t) \quad (14)$$
$$+(a_1\frac{(a_2+\sqrt{a_3+x_0})}{\sqrt{a_2+x_0}}(-\frac{\tau_1+\tau_2}{\tau_1 s+1}\frac{dx_0}{d\alpha})\, sin\,\alpha_0 + C_{Lq}^{fo}\frac{c}{V})(\alpha_s\omega\, cos\,\omega\, t)$$

Meanwhile, for harmonic oscillations, the aerodynamic coefficient can be written as follows:

$$C_L^{nl}(\alpha,x) = (C_{L0}^{nl} + C_{L\alpha}^{fo}\alpha + C_{L\dot{\alpha}}^{fo}\dot{\alpha}) \quad (15)$$

And by comparison of similar $(\tau_1 s+1)$ components in eqns. (14) and (15), the relations between dynamic derivatives and time characteristics can be derived:

$$\begin{cases} C_{L\dot{\alpha}}^{fo} = -\left(a_1\frac{(a_2+\sqrt{x_0+a_3})}{\sqrt{x_0+a_3}}sin\,\alpha_0\right)\frac{(\tau_1+\tau_2)}{1+{\tau_1}^2\omega^2}\frac{dx_0}{d\alpha} \\ C_{L\alpha}^{fo} = a_1\left[(a_2+\sqrt{x_0+a_3})^2+a_4\right]cos\,\alpha_0 - \left(a_1\frac{(a_2+\sqrt{x_0+a_3})}{\sqrt{x_0+a_3}}sin\,\alpha_0\right)\frac{(\tau_1+\tau_2)\tau_1\omega^2}{1+{\tau_1}^2\omega^2}\frac{dx_0}{d\alpha} \end{cases} \quad (16)$$

Since the relations have been determined through equation derivation, the next step is to obtain the value of dynamic derivatives $C_{L\dot{\alpha}}^{fo}$and $C_{L\alpha}^{fo}$.

Static aerodynamic derivatives obtained from static wind tunnel testing can yield the dominant characteristics of the aircraft motion about trim conditions. Meanwhile, the damping derivatives are required for accurately describing maneuver flight, especially at stall and post-stall angles-of-attack region. Therefore, forced dynamic wind tunnel experiments are used to determine damping derivatives. Traditional forced oscillation is not feasible on the maneuver rig although two alternative forced oscillation approaches can be implemented: forced oscillation induced by the model control surface actuators and oscillations forced by the compensator control surfaces. It is also possible to induce free oscillations. For the first alternative method, the model is configured on the rig with one degree of freedom (pitch) and a sine trigonometric-function voltage signal was transmitted to longitudinal actuator, i.e. elevator (for the Hawk this is an all moving horizontal tail) through the wireless data transmission setup. The horizontal tail deflection then has approximately the same amplitude and frequency as the input signal. Dynamic characteristic of the model response with this signal input were recorded over a few periods of motion and dynamic derivatives extracted from the measured data in the usual manner. Note that the oscillation frequency is normalized into the dimensionless similarity parameter (reduced frequency) [30-33]: $k = \pi f c/V$

This is typically done in order to ensure equivalence to a full-scale air vehicle, with the actual wind tunnel test frequency determined accordingly. For small scale models, dynamic wind tunnel experiments must meet higher frequency requirements than in full scale and the equipment must be capable of achieving adequate measurement accuracy under these conditions. Whilst the maneuver rig equipment does meet these forced oscillation test requirements, the values of $\tau_1$and $\tau_2$have been deduced here through an alternative approach, namely from experiments in which the motions are obtained via limit cycle oscillations. The initial values of $\tau_1$and τ_2 were based on past experience with the model data. The genetic algorithm combined with the bifurcation analysis plot can be used to identify model parameters. First, the two time constants $\tau_1$and τ_2 are looked as variables to be optimized. Then the results of the bifurcation analysis and the wind tunnel test will be as consistent as possible through the given coding strategy and the genetic strategy, i.e. the error between the results will get smaller as the progress of the genetic algorithm. From observing wind tunnel test results, we found there are four key points: limit cycle starting point, ending point and a pair of 'jump' points respectively. To some extent, the characteristics of the limit cycle will be determined by these points. For this reason, the objective function is defined to minimize the sum of the squares of the offsets of the points between experimental results and bifurcation analysis results. In the numerical simulation, the initial population size is set to 10. Then the optimal time constants which are $\tau_1 = 42.2$, $\tau_2 = 3.15$ respectively , are obtained after 50 generations of genetic optimization

5. Bifurcation Analysis

A numerical continuation package was used to find the bifurcation diagram of the numerical model. Bifurcation analysis is a powerful method for studying steady-state nonlinear dynamic systems. Software tools make it possible to generate 'maps of solutions' in an efficient way that provide valuable insight into the overall dynamic behaviour of a system[34] . Since an aircraft system is a typical dynamic system, the application of bifurcation analysis has already been employed in some aircraft studies. In this section, this tool will be used to analyse dynamic characteristics of the Hawk model, with the aerodynamic models built in sections III and IV. Matlab COCO[35] is the numerical continuation software adopted in this study.

When investigating stability and control, handling qualities and performance issues, the aircraft is usually considered as a rigid-body six degree-of-freedom system in which the inertial reference is a point on a non-rotating earth axes[35-37]. For stability and control studies, the position and heading angle relative to the Earth can be ignored, and height may be regarded as constant[37]. This yields an 8th order system and equations (17) are a typical form of flight dynamics equations used for stability and control studies. The eight first-order ordinary differential equations relate forces and moments to aircraft motion and orientation[37, 40]. Because lateral and directional freedom were locked in the test, and unsteady effect was take into account, so the 8th order equations become 3th order, equations(18).

$$\dot{V} = \frac{1}{m}\begin{bmatrix} T\cos\alpha\cos\beta - \bar{q}S(C_D\cos\beta - C_Y\sin\beta) \\ -mg\sin\gamma \end{bmatrix} \tag{17}$$

$$\dot{\alpha} = q - \frac{1}{\cos\beta}\begin{bmatrix} (p\cos\alpha + r\sin\alpha)\sin\beta \\ -\frac{g}{V}\cos\gamma\cos\mu + \frac{\bar{q}SC_L}{mV} + \frac{T\sin\alpha}{mV} \end{bmatrix}$$

$$\dot{\beta} = (p\sin\alpha - r\cos\alpha) + \frac{1}{mV}\begin{bmatrix} -T\cos\alpha\sin\beta + \\ \bar{q}S(C_Y\cos\beta + C_D\sin\beta) + mg\cos\gamma\sin\mu \end{bmatrix}$$

$$\dot{p} = \frac{1}{2I_{xx}}\rho V^2 SbC_l + (\frac{I_{yy} - I_{zz}}{I_{xx}})qr$$

$$\dot{q} = \frac{1}{2I_{yy}}\rho V^2 ScC_m + (\frac{I_{zz} - I_{xx}}{I_{yy}})pr$$

$$\dot{r} = \frac{1}{2I_{zz}}\rho V^2 SbC_n + (\frac{I_{xx} - I_{yy}}{I_{zz}})pq$$

$$\dot{\phi} = p + q\sin\phi\tan\theta + r\cos\phi\tan\theta$$

$$\dot{\theta} = q\cos\phi - r\sin\phi$$

$$\dot{\alpha} = q - \frac{1}{\cos\beta}\begin{bmatrix} (p\cos\alpha + r\sin\alpha)\sin\beta \\ -\frac{g}{V}\cos\gamma\cos\mu + \frac{\bar{q}SC_L}{mV} + \frac{T\sin\alpha}{mV} \end{bmatrix} \tag{18}$$

$$\dot{q} = \frac{1}{2I_{yy}}\rho V^2 ScC_m + (\frac{I_{zz} - I_{xx}}{I_{yy}})pr$$

$$\dot{x} = (x_0(\alpha - \tau_2\dot{\alpha}) - x)/\tau_1$$

For stability analysis, parametric continuation methods are used to solve the equations numerically for their steady states – equilibria and limit cycles – and associated local stability. The solutions are usually presented as bifurcation diagrams and it is possible to present experimental results in this form too (although only stable steady states are available from conventional testing).

A 1-DOF (model pitch) longitudinal experiment is first conducted in the wind tunnel (model yaw and roll gimbal axes locked and rig arm gimbal locked in all axes). The test is carried out at a wind speed of $30m/s$. Figure. 6 shows a one-parameter bifurcation diagram extracted from time histories; it depicts equilibria and estimated minima and maxima of limit cycle steady states in the model-pitch angle θ_m projection and with the elevator input δ_e. Note that θ_m is equivalent to α_m in this 1-DOF test, and that the minima and maxima of the limit cycle amplitudes are estimated by extracting data for

which $|\dot{\alpha}|$ is close to zero. The initial condition for this test is $\delta_e = -1.6°$,$\alpha = 5.0°$, and$q = 0.0^{\circ}/s$, corresponding to a trim condition. In this process, elevator changes from the initial value to a final value ($\delta_e = -29°$) then back, with a very slow rate of change of elevator. This allows the test results to be considered as quasi-steady.

Figure. 6 shows that limit cycles occur in the region delimited by $-11° < \delta_e < -23°$. In order to observe the limit cycle responses more clearly, Figure.7 shows the limit cycle phase portrait with different elevator inputs. This demonstrates that these motions are indeed limit cycle oscillations.

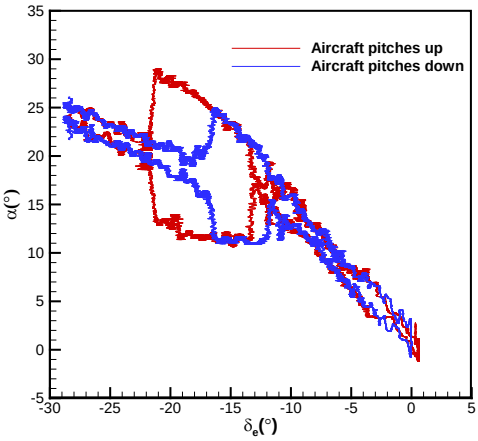

Figure 6 –1-DOF Hawk model pitch smoothed experimental bifurcation diagram at a wind speed of 30m/s.

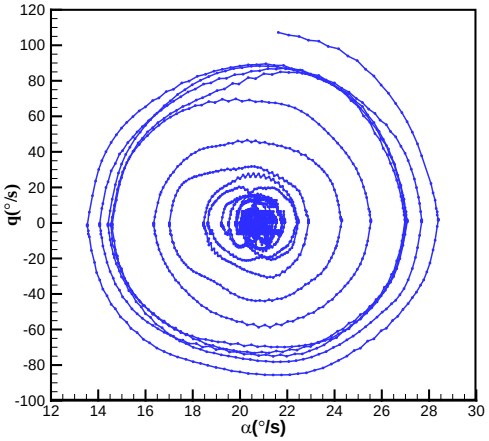

Figure 7 –1-DOF aircraft model pitch limit cycle phase portraits

The LCO regions occur at moderate to high α. A clear difference in the aircraft pitch angle response can be observed when comparing the plot corresponding to the model pitching up motion (red line) with the one corresponding to the aircraft model pitching down motion (blue line). This difference in response could be indicative of flow detachment over the wing and is an example of aerodynamic hysteretic behavior[24]. The corresponding physical interpretation is that the model maintains trim conditions with absolute value of elevator increasing; when elevator reaches approximately $-11°$, model begins to oscillate around the trim angle. This oscillation is another form of stability and is defined as a stable limit cycle oscillation. Its amplitude grows with increasing elevator, until $\delta_e \approx -21°$, after which the oscillations suddenly cease in favour of the non-oscillatory stable trim (note that the non-zero amplitudes evident in Figure. 6 in the low and high α stable trim regions reflect tunnel turbulence effects). For the pitch down situation, the model keeps on the stable trim solution branch with elevator absolute value decreasing until the elevator reaches approximately $-19°$; here, the model begins oscillating around the unseen unstable trim solutions. Its amplitude becomes smaller with decreasing elevator until, when $\delta_e \approx -12°$, the LCO disappears.

The flight dynamics differential equations (17) were then applied to reflect the behavior corresponding to this 1-DOF experiment. The aerodynamic model established in section IV was used in this process. All force components, along with yaw and roll moments, are neglected in (17), as those DOFs were locked in the experiment. The pitching moment coefficient is $C_m = C_m^{nl}(\alpha, x) + C_{mq}^{att}\frac{qc}{V} + C_{m\dot{\alpha}}^{att}\frac{\dot{\alpha}c}{V} + C_{mde}\delta_e$

Through solving the equations for equilibria and LCO steady states using COCO, the two 1-parameter bifurcation diagrams (one for decreasing and one for increasing elevator deflection) can be seen in Figure. 8 and Figure. 9 respectively. The corresponding experimental data are shown for comparison. In these Figures, the orange line denotes experimental results and the others represent the computed bifurcation analysis. The equilibria and maximum amplitude of the limit cycle are shown together with the identified bifurcation points (red circles). In the Figures, the green line with blue triangles denotes stable equilibria, the green line with red dots unstable equilibria, the blue dots stable LCO, pink dots unstable LCO and black stars denotes saddle points.

It is evident that the computed bifurcation diagram captures the main characteristics of the LCO observed in the wind tunnel tests. For the decreasing elevator direction, i.e. elevator changes from

right to left in Figure. 8, when the elevator reaches $-10°$ the model encounters a Hopf bifurcation in which the equilibria lose stability and a stable limit cycle oscillation arises (blue dots). It develops in amplitude with decreasing elevator until $\delta_e \approx -21°$, where the stable LCO folds back and no longer exists. The solution therefore 'jumps' back to the (re-stabilised) equilibrium branch, corresponding to the aircraft model oscillations disappearing rapidly.

On the other side, for increasing elevator, i.e. elevator changes from left to right in Figure. 9, when it reaches $-18°$ the model enters a large amplitude stable LCO (blue dots) from the higher-α equilibrium solution branch. Once in the LCO, the amplitude gradually decreases with increasing elevator, until $\delta_e \approx -12°$at which point the LCO disappears completely, and the system returns to an equilibrium situation.

Figure. 8 and Figure. 9 show that the numerical bifurcation diagrams using the Goman-Khrabrov state space modelling of pitching moment capture the main features of the LCO hysteretic behaviour from the two elevator history directions, although not a perfect match.

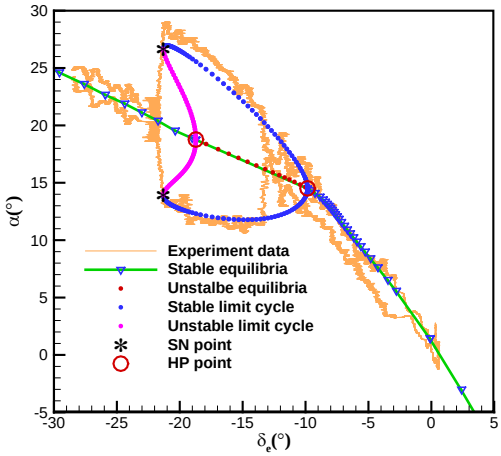

Figure 8 – 1-DOF bifurcation diagram comparing with model pitching up motion.

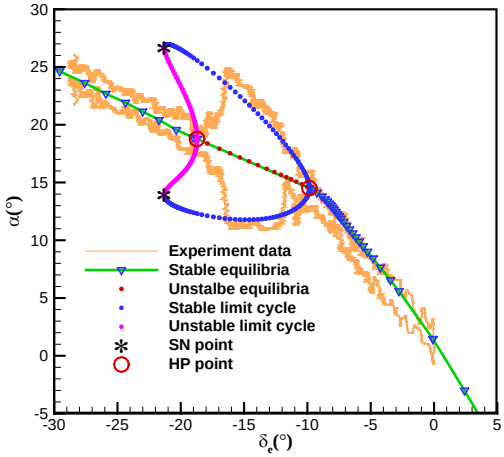

Figure 9 – 1-DOF bifurcation diagram comparing with model pitching down motion

Time-history simulation (Figure.10 and Figure.11) has also been conducted to investigate the frequency of the LCO. The results showed that, both the amplitude and frequency of the LCO obtaining from simulation match well with the experiment result. It further proves that the modelling method used in this paper could capture not only the amplitude features of LCO but also the frequency features.

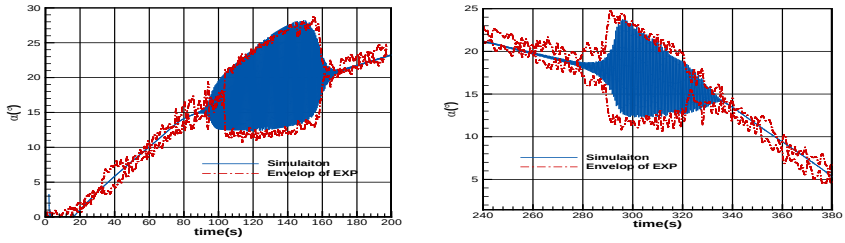

Figure 10 – Comparison of time-history simulation and experiment result

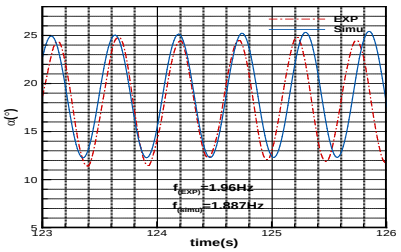

Figure 11 – Comparison of frequency of the LCO.

The variation of separation points with different elevator input ramp rates is shown in Figure. 13. The trend is in accordance with conclusions in section III, which is that unsteady effects will postpone flow separation with $\dot{\alpha} > 0$, and will bring forward flow separation with$\dot{\alpha} < 0$. In addition, with ramp rate growing positively, LCO envelopes will become bigger and even diverge, whilst LCO envelopes will become smaller, and even disappear, with ramp decreasing.

τ_1 and τ_2 also have significant effects on LCO properties. LCO with different characteristic times are shown in Figure. 14. Blue lines mean stable equilibria, red dots unstable equilibria and green dotted lines the minimum and maximum amplitudes of stable LCO. Orange lines denote min. and max.

amplitudes of unstable LCO, red circles denote Hopf points and black stars denotes saddle points. For exploring the influence of τ_1 and τ_2, further bifurcation analysis tests have been done. Figure. 14 gives the analysis results with τ_2 changing. When τ_1 is fixed, LCO will become bigger and even diverge with increasing τ_2.On the contrary, with fixedτ_1,LCO will become smaller and eventually disappear with decreasing τ_2.

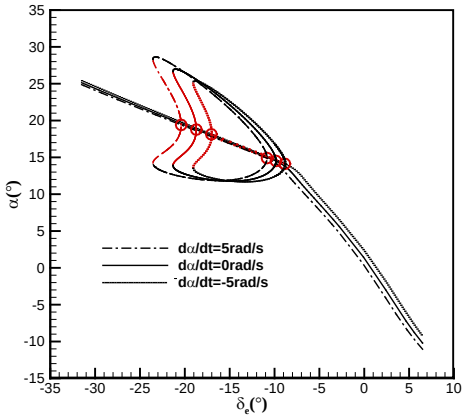

Figure 12 – 1-DOF bifurcation diagram with different elevator input ramp rates.

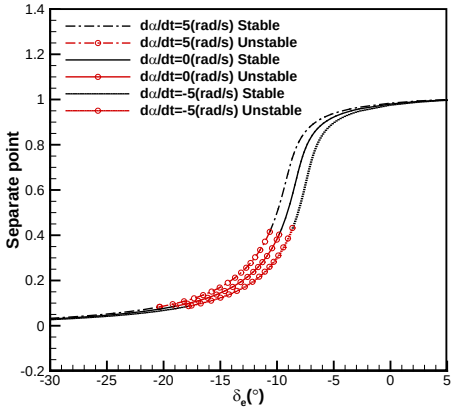

Figure 13 – Separation positions with different elevator input ramp rate:$\dot{\alpha}_1 = -5\mathrm{rad/s}$, $\dot{\alpha}_2 = 0\mathrm{rad/s}$, $\dot{\alpha}_3 = 5\mathrm{rad/s}$ ($\tau_1 = 42.2$, $\tau_2 = 3.15$).

Taking a close-up view, there are still unstable parts (orange lines) in some sections of LCO. The relevant diagrams are given in Figure. 14 (1.a), (1.b) and (1.c). In Figure. 14, blue points with blue line means stable equilibria, red points with blue line means unstable equilibria, green points means stable limit cycle, orange line means unstable limit cycle, red circles means HP points and black stars means SN points. Noting that there are two Hopf points for each diagram, with an LCO appearing between them, see observe that if the distance between limit cycles becomes bigger, the gap between two Hopf points also becomes longer. The exact locations of Hopf points with different characteristic times can be seen in Table 2.

Table 2 – The value of elevator (degree) at Hopf points.

	Figure. 14	**Figure. 14**	**Figure. 14**
(1)	(-18.72, -9.84)	(-19.68, -9.73)	(-20.56, -9.66)
(2)	(-17.19,-10.05)	(-18.72, -9.84)	(-18.72, -9.84)
(3)	(-15.13, -10.5)	(-17.3, -10.05)	(-15.38, -10.45)

Furthermore, when τ_2 is fixed, the LCO will diminish and disappear with increasing τ_1 and the LCO will enlarge and diverge with decreasing τ_1. The effects of dynamic characteristics of the aircraft model also were investigated. Longitudinal dynamic derivative C_{mq} is an important parameter which represents the pitch damping of the aircraft. A negative value of C_{mq} means the aircraft has longitudinal dynamic stability; otherwise it is dynamically unstable. Therefore, an inference can be made that an LCO will enlarge and diverge with decreasing dynamic stability, and will diminish and even disappear with increasing dynamic stability. Analysis results (not shown) are consistent with this inference.

From these studies, the effects of the parameters of the dynamic system have been gained. From a flight safety perspective, appropriate combinations of parameters can be chosen to avoid upset – either by modifying the geometry of the aircraft in early design stages or by augmenting stability derivatives using feedback control.

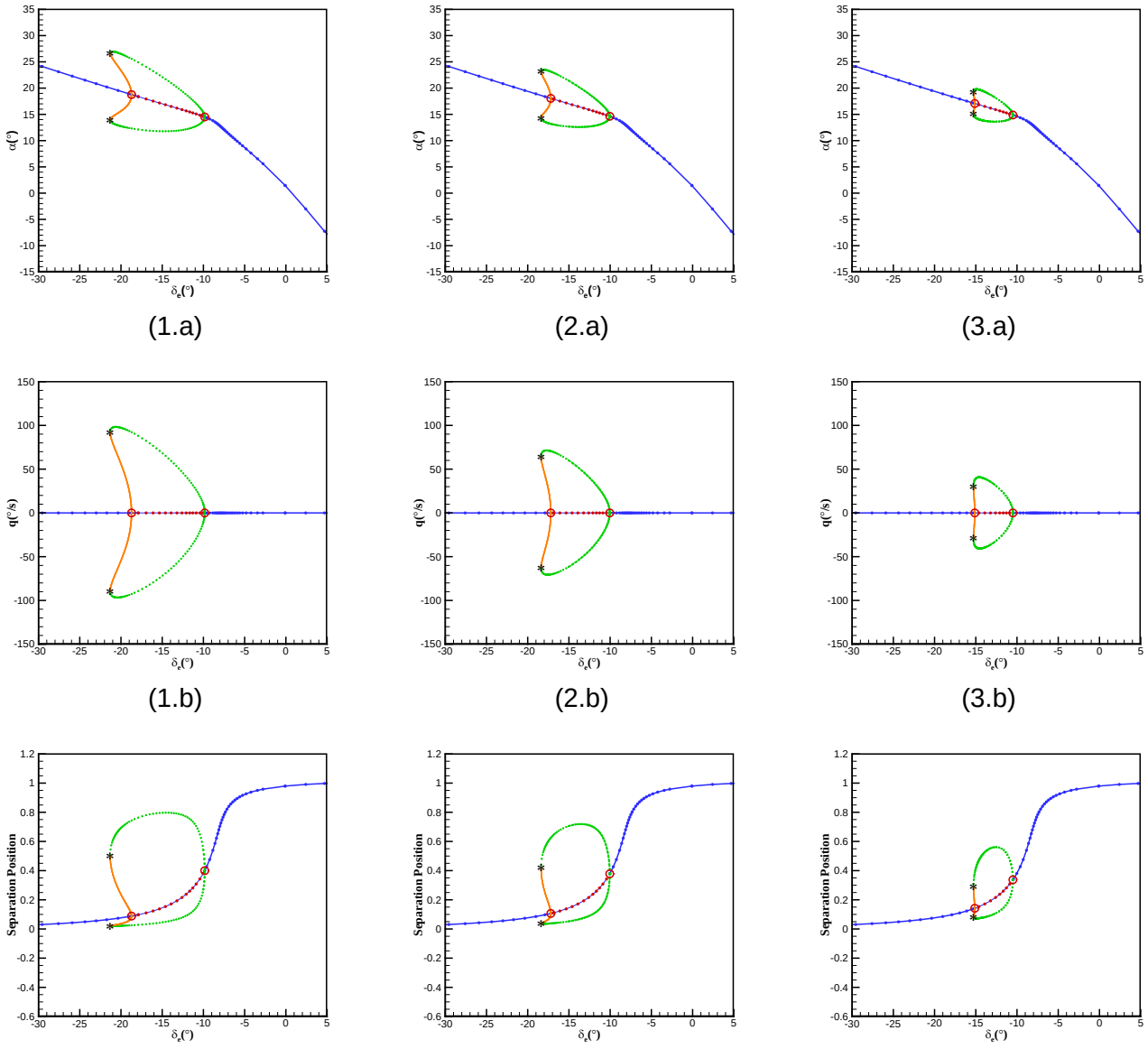

(1.a) (2.a) (3.a)

(1.b) (2.b) (3.b)

(1.c) $\tau_1 = 42.2, \tau_2 = 4.15$ (2.c) $\tau_1 = 42.2, \tau_2 = 3.15$ (3.c) $\tau_1 = 42.2, \tau_2 = 1.5$

Figure 14 – One-DOF bifurcation diagram with different τ_2

6. Conclusions

This paper considers a new approach to the modelling of aerodynamics of a sub-scale aircraft configuration for which a physical wind tunnel model exhibits limit cycle oscillations in pitch due to unsteady separation flow phenomena. The method combines a Goman-Khrabrov state-space model formulation with bifurcation analysis. The G-K model takes unsteady aerodynamics into account through a generalized internal state variable, representing a notional separation point position. The state-space format allows this to be appended to the aircraft equations of motion, providing a powerful tool for the study of nonlinear and unsteady problems. A bifurcation analysis of the system reveals the interesting hysteretic limit cycle phenomenon with multiple stable solutions in certain elevator ranges (corresponding to certain angle-of-attack ranges). It is shown in the paper that the aerodynamic state-space model of the pitching behaviour permits the bifurcation analysis to achieve a good qualitative match to the experimental results(not only stability characteristics, but also amplitude and frequency features of LCO). The characteristic times used in the modeling (relating to

dynamic characteristics of

the aircraft) were found to affect the shape and onset of LCO. Variations in elevator input rate and in the pitch damping derivative were also seen to impact on the limit cycle behavior.

Although there are limitations in the analysis process, the method presented in the paper does reveal some inherent dynamic features of the aircraft responses. By comparing previous research, the mathematical model developed here is more general than before and allows for a more direct physical interpretation of the influence of the model parameters.

There remain several developments worth pursuing in ongoing research:

- Expand experiment degrees of freedom. Only 1-DOF test and bifurcation analysis are reported above. To get more general results, more of the 5 maneuver rig degrees of freedom should be freed: yaw, roll, heave and sway. In addition, the aircraft model behavior is coupled to the rig arm and compensator, and these effects should be considered in the modeling process.
- The LCO is sensitive to characteristic time parameters: study of the relations between LCO and these parameters could be useful to ensure better prediction of the LCO shape and onset points.
- Alternative ways to establish an unsteady aerodynamic model could be explored.
- For practical use, this analysis method could be tested on a wider range of aircraft models

References

[1] Davison, P. M., Lowenberg, M. H., and di Bernardo, M., "Experimental Analysis and Modeling of Limit Cycles in a Dynamic Wind-Tunnel Rig, " *Journal of Aircraft*, Vol. 40, No. 4, 2003, pp. 776-785.doi: 10.2514/2.3158

[2] Davison, P. M., di Bernardo, M., and Lowenberg, M. H., "Modeling and Control of a Single Degree-of-Freedom Dynamic Wind Tunnel Rig, " *2003 European Control Conference (ECC)*, Cambridge, UK, 1-4 Sep. 2003.

[3] Belcastro , C. M., Khong, T. H., Shin, J., Kwatny, H., Chang, B., and Balas, G. J., "Uncertainty Modeling for Robustness Analysis of Aircraft Control Upset Prevention and Recovery Systems, " *AIAA Atmospheric Flight Mechanics Conference and Exhibit*, San Francisco, California, AIAA-2005-6427, Aug. 2005.

[4] Cunningham, K., Foster, J. V., Morelli, E. A., and Murch, A. M., "Practical application of a subscale transport aircraft for flight research in control upset and failure conditions, " *AIAA Atmospheric Flight Mechanics Conference and Exhibit*, Honolulu, Hawaii, AIAA-2008-6200, Aug. 2008.

[5] Araujo-Estrada, S. A., and Lowenberg, M. H., "Evaluation of Aircraft Model Upset Behaviour Using Wind Tunnel Manoeuvre Rig, " *AIAA Atmospheric Flight Mechanics Conference*, AIAA 2015-0750, Jan. 2015.

[6] Kyle, H., "An Investigation into the use of a Pendulum Support Rig for Aerodynamic Modeling," Ph.D. Dissertation, Department of Aerospace Engineering, Faculty of Engineering, University of Bristol, 2004.

[7] Pattinson, J., Lowenberg, M. H., and Goman, M. G., "A Multi-Degree-of-Freedom Rig for the Wind Tunnel Determination of Dynamic Data, " *AIAA Atmospheric Flight Mechanics Conference*, AIAA 2009-5727, 2009.

[8] Pattinson, J., "Development and evaluation of a wind tunnel manoeuvre rig," Ph.D. Dissertation, Department of Aerospace Engineering, Faculty of Engineering, University of Bristol, 2010.

[9] Pattinson, J., Lowenberg, M. H., and Goman, M. G., "Multi-Degree-of-Freedom Wind-Tunnel Maneuver Rig for Dynamic Simulation and Aerodynamic Model Identification," *Journal of Aircraft*, Vol. 50, No. 2, 2013, pp. 551-566. doi: 10.2514/1.C031924

[10] Pattinson, J., Lowenberg, M. H., and Goman, M. G., "Investigation of Poststall Pitch Oscillations of an Aircraft Wind-Tunnel Model, " Journal of Aircraft, Vol. 50, No. 6, 2013, pp. 1843-1855.doi: 10.2514/1.C032184

[11] Navaratna, P. D. B., Lowenberg, M. H., and Neild, S. A., "Minimally-constrained flight simulation in a wind tunnel, " *J. Aircraft*, published online Jan. 2019. doi: 10.2514/1.C035199

[12] Goman, M. G., and Khrabrov, A. N., "State-Space Representation of Aerodynamic Characteristics of an Aircraft at High Angles of Attack, " *Journal of Aircraft*, Vol. 31, No. 5, pp.1109-1115, 1994.

[13] Rajamurthy, M. S., "Generation of comprehensive longitudinal aerodynamic data using dynamic wind tunnel simulation, " *Journal of Aircraft*, Vol. 34, No. 1, 1997, pp. 29-33.

[14] Peyada, N. K., Gosh, A. K., and Go, M., "Mathematical modelling, simulation, and estimation of aircraft parameters using five degree-of-freedom dynamic test rig," *Proceedings of the Institution of Mechanical Engineers*, *Part G: Journal of Aerospace Engineering*, Vol. 226, No. 1, 2012, pp. 55–63.doi: 10.1177/0954410011407265

[15] Owens, D. B., Brandon, J. M., Croom, M. A., Fremaux, C. M., Heim, E. H., and Vicroy, D. D., "Overview of Dynamic Test Techniques for Flight Dynamics Research at NASA LaRC," AIAA-2006-3146, 25th AIAA Aerodynamic Measurement Technology & Ground Testing Conference, Jun. 2006.

[16] Huang, X. Z., Lou, H. Y., and Hanff, E. S., "Nonlinear indicial response and internal state-space representation for free-to-roll trajectory prediction of 65º delta wing at high incidence, " AIAA 2002-4713[R]. Reston: AIAA, 2002.

[17] Hall, R. M., Woodson, S. H., and Chambers, J. R., "Overview of the abrupt wing stall program," *Progress in Aerospace Sciences*, Vol. 40, pp. 419-452, 2004.

[18] Williams, D. R., An, X., Iliev, S., King, R., and ReiBner, F., "Dynamic hysteresis control of lift on a pitching wing," *Exp Fluids* (2015) 56:112.doi: 10.1007/s00348-015-1982-y

[19] Fischenberg, D., "Identification of an unsteady aerodynamic stall model from flight test data," AIAA 95-3438[R]. Reston: AIAA, 1995.

[20] Sing, J., and Jategaonkar, R. V., "Flight determination of configurational effects on aircraft stall behaviour," AIAA 96-3441[R], Reston: AIAA, 1996.

[21] Fan, Y. G., and Lutze, F. H., "Identification of an unsteady aerodynamic model at high angles of attack." AIAA 96-3407, Reston: AIAA 1996.

[22]Lutze, F. H., Fan, Y. G., and Stagg, G., “Multiaxis unsteady aerodynamic characteristics of an aircraft.” AIAA 99-4011[R], Reston: AIAA, 1999.

[23]Pashilkar, A. A., Pradeep, S., “Unsteady aerodynamic modelling using multivariate orthogonal polynomials.” AIAA 99-4014[R], Reston: AIAA 1999

[24]Abramov, N. B., Goman, M. G., Greenwell, D. I., and Khrabrov, A. N., “Two-step linear regression method for identification of high incidence unsteady model.” AIAA 2001-4080[R].

[25]Abramov, N., Goman, M., Khrabrov, A., Kolesnikov, E., Sidoruk, M., Soemarwoto, B., and Smaili, H., “Aerodynamic Model of Transport Airplane in Extended Envelope for Simulation of Upset Recovery.” 28th International Congress of the Aeronautical Sciences, 2012.

[26]Araujo-Estrada, S. A., “Control of a Wind Tunnel Manoeuvre-Rig to Physically Simulate Free-Flight Motion of an Aircraft Model, ” Ph.D. Dissertation, Department of Aerospace Engineering, Faculty of Engineering, University of Bristol, 2016.

[27]Araujo-Estrada, S. A., Gong, Z., Lowenberg, M. H., Neild, S., and Goman, M., “Wind Tunnel Manoeuvre Rig: A Multi-DOF Test Platform for Model Aircraft,” AIAA 2016-2119, AIAA SciTech Conf., Jan 2016.

[28]Gong, Z., Araujo-Estrada, S., Lowenberg, M., Neild S., and Goman, M., “Experimental Investigation of Aerodynamic Hysteresis Using a Five-Degree-of-Freedom Wind-Tunnel Maneuver Rig, ” Journal of Aircraft, published online, Jan. 2019. doi: 10.2514/1.C034995

[29]Gurevitch, M. L., *Theory of Ideal Fluids Jets (in Russian)*, Nauka, Moscow, 1979.

[30]Petoshin, V. I., and Chasovnikov, E. A., “Aerodynamic Characteristics of Passenger and Transport Aircraft Models at Harmonic Oscillations on the Pitch Angle for High Angles of Attack,” *Thermophysics and Aeromechanics*, Vol. 18, No. 3, pp359-368, 2011.

[31]Klein, V., Murphy, P. C., and Szyba, N. M., “Analysis of Wind Tunnel Lateral Oscillatory Data of the F-16XL Aircraft.” NASA/TM-2004-213246, Jul. 2004.

[32]Hoe, G., Owens, D. B., and Denham, C., “Forced Oscillation Wind Tunnel Testing for FASER Flight Research Aircraft,” *AIAA Atmospheric Flight Mechanics Conference*, AIAA 2012-4645, 2012.

[33]Burt, G. E., “Forced-Oscillation Test Mechanism for Measuring Dynamic Stability Derivatives in Roll.” *J. Aircraft*. 11-17. Vol.12. No.1, January 1975.

[34]Sharma, S., Coetzee, E. B., Lowenberg, M. H., Neild, S. A., and Krauskopf, B., “Numerical Continuation and Bifurcation Analysis in Aircraft Design: An Industrial Perspective. Philosophical Transactions A: Mathematical,” *Physical and Engineering Sciences*, 373(2051), 2015.

[35]Dankowicz, H., and Schilder, F., 2013 Recipes for continuation.Philadelphia, PA: Society for Industrial and Applied Mathematics. Continuation Core and Toolboxes (COCO). http://sourceforge.net/projects/cocotools/?source=directory.

[36]Smith, A. P., Crespo, L. G., Munoz, C. A., and Lowenberg, M. H., “Bifurcation Analysis Using Rigorous Branch and Bound Methods,” 2014 IEEE Int. Conf. on Control Applications (CCA), Part of 2014 IEEE Multi-conference on Systems and Control, Antibes, France, Oct. 2014, pp. 2095–2100.

[37]Lowenberg, M. H., “Bifurcation Analysis of Multiple-Attractor Flight Dynamics,” Philosophical Transactions: Mathematical, Physical and Engineering Sciences, Vol. 356, No. 1745, Nonlinear Flight Dynamics of High-Performance Aircraft, pp. 2297-2319, Oct. 1998.

[38]Sinha, N. K., and Ananthkrishnan, N., “Elementary Flight Dynamics with an Introduction to Bifurcation and Continuation Methods, ” CRC Press, 2013.

[39]Carroll, J. V., and Mehra, R. K., “Bifurcation Analysis of Nonlinear Aircraft Dynamics, Journal of Guidance,” Control and Dynamics, Vol. 5, No. 5, 1982, pp. 1225-1228.

[40]Navaratna, P. D. B., “Correcting Froude Number Mismatch Using A Multi-Degree-of-freedom maneuver rig, ” Department of Aerospace Engineering, Faculty of Engineering, University of Bristol,2011.

Copyright Statement